Ceramics International 45 (2019) 10572–10580

Contents lists available at ScienceDirect

Ceramics International

journal homepage: www.elsevier.com/locate/ceramint

Achieving carbon-rich silicon-containing ceramic anode for advanced lithium ion battery☆

Muhammad Idrees[a], Saima Batool[a], Qiang Zhuang[a], Jie Kong[a,**], Ilwoo Seok[e], Jiaoxia Zhang[b,d], Hu Liu[b,f], Vignesh Murugadoss[b], Qiang Gao[c,***], Zhanhu Guo[b,*]

[a] MOE Key Laboratory of Materials Physics and Chemistry in Extraordinary Conditions, Shaanxi Key Laboratory of Macromolecular Science and Technology, School of Natural & Applied Sciences, Northwestern Polytechnical University, Xi'an, 710072, China
[b] Integrated Composites Laboratory (ICL), Department of Chemical and Biomolecular Engineering, University of Tennessee, Knoxville, TN, 37996, USA
[c] Scanning Probe Microscopy Group, Center for Nanophase Materials Sciences, Oak Ridge National Laboratory, P.O. Box 2008, Oak Ridge, TN, 37831, USA
[d] College of Material Science and Engineering, Jiangsu University of Science and Technology, Zhenjiang, 212003, Jiangsu Province, China
[e] Mechanical Engineering, Arkansas State University, PO Box 1740, State University, AR, 72467, USA
[f] Key Laboratory of Materials Processing and Mold (Zhengzhou University), Ministry of Education, National Engineering Research Center for Advanced Polymer Processing Technology, Zhengzhou University, Zhengzhou, 450002, China

ARTICLE INFO

Keywords:
Lithium-ion batteries
Electrochemical cycling
High capacity
Si/C anode

ABSTRACT

Silicon carbon (Si/C) materials are promising anode candidates for high performance lithium ion batteries (LIBs). However, serious volume expansion and solid electrolyte interface formation limited their actual capacity during lithiation and delithiation. In the present study, an innovative and low-cost synthetic approach was developed for synthesizing carbon-rich silicon-containing polymer-derived ceramics from poly(dimethylsilyene) diacetylenes (PDSDA) and its feasibility to be used as anodes was demonstrated. The attained PDCs@800 °C exhibited a high specific capacity upto 883 $mAhg^{-1}$ at 400 mAg^{-1}, with > 99% coulombic efficiency (CE), and 90% capacity retention even after 500 cycles, setting a new record for PDCanode materials in LIBs. The high specific capacity was attributed to the incessant Si/C network which delivered consistent conductance and a stable solid electrolyte interphase (SEI). This study opens the door to explore and apply well-designed ceramic materials derived from tailored polymers as high performance anodes for lithium ion batteries.

1. Introduction

The rapidly developing portable electronics and electric vehicles demand lighter, safer and high capacity lithium ion batteries (LIBs). Silicon has emerged as an appealling anode for LIBs due to its high theoretical capacity (~4200 $mAhg^{-1}$) [1]. Unfortunately, the silicon electrodes suffer from a severe pulverization by volume expansion (~280%) during lithiation and delithiation, yielding a fast capacity loss in the first few cycles [2,3]. Various approaches have been explored to circumvent the stability issues by forming structured Si electrodes including thin films, micro- and nano-sized particles as well as composites [4]. Highly interconnected Si nanowires prevent individual nanowires to detach from the substrate to improve the cyling stability [4]. Active Si nanotube surrounded by an ion-permeable Si shell have been developed to operate over 6, 000 cycles with more than 85% remaining of their initial capacity [5]. The outer surface was protected from expansion by the oxide shell, and the expanding inner surface was not exposed to the electrolyte, achieving a stable solid electrolyte interphase (SEI). Si-nanolayer-embedded graphite/carbon anode structure presents a high-first-cycle efficiency up to 92% and a rapid efficiency increases to 99.5% after only 6 cycles, yielding a capaicty retention of 96% after 100 cycles [6]. Choi and Park et al. have reported a Si-based

* Corresponding author.
** Corresponding author.
*** Corresponding author.
E-mail addresses: kongjie@nwpu.edu.cn (J. Kong), gaoq@ornl.gov (Q. Gao), zguo10@utk.edu (Z. Guo).

https://doi.org/10.1016/j.ceramint.2019.02.123
Received 14 February 2019; Received in revised form 17 February 2019; Accepted 18 February 2019
Available online 19 February 2019

porous composite with high stability [7]. A micro-sized carbon coated Si-based multicomponent including Si/SiO cores and crystalline SiO_2 shells has demonstrated a high reversible capacity with a remarkable durability [8]. The influence of Si building block size for Si-C composites has revealed a critical size of 15 nm to achieve high stability and capacity sponteneously [9].

In a continuous search for solving the capacity degradation, Si-based polymer derived ceramics (PDCs), namely silicon oxy-carbides (SiOC) or silicon carbon nitrides (SiCN), have been stuided and showed a higher resistance to crystallization and possessed amorphous carbons [10–12]. These materials outperform the widely used graphite in terms of capacity and high rate performance [13–20], undergoing less degrees of volume expansion compared with Si anodes [21,22]. Halim et al. synthesized SiOC anode using phenyl-rich silicone oil precursor and the resulting sample demonstrated the stability up to 250 cycles with 800 mAh g^{-1} capacity at 200 mA g^{-1}, owing to its extremely low volume change and relatively fast lithium ion mobility with the matrix [23]. David et al. demonstrated a freestanding SiOC in rGO matrix anode with a 588 mAh g^{-1} capacity during 1020 cycles without showing noticeable mechanical failure [23]. The porous rGO matrix played an important role as electron conductor and current collector with a stable mechnical structure, whereas SiOC cycled the Li^+ with high Coulombic efficiency. Vrankovic et al. synthesized Si/C/SiOC composites to provide ~600 mAh g^{-1} with almost no capcity decay up to 100 cycles [24]. The promising performance arises from three folds: i) accommodation of the volume changes during lithiation in the open porosity; ii) high conductivity due to the existence of carbon; iii) encapsulation of the SiOC favoring the adaption of volume changes and minimizing the SEI formation. Regarding the SiCN-based composites, Graczyk-Zajac et al. reported endurable SiCN/graphite composite anodes, exhibiting a higher capacity than that of the sum of both components [25]. The remarakble stability arose from the presence of the SiCN ceramic phase. Feng et al. synthesized anodes from controlled pyrolysis of poly(silylcarbondiimide) to realize 722.4 mAh g^{-1} capacity at the first cyelc and 475.1 mAh g^{-1} after 100 cycles [26]. High rate peformance was achieved with 800 mA g^{-1} and a capacity as high as 260 mAh g^{-1}. Typically, the Si-based PDCs were prepared by controlled pyrolysis. For example, Riedel et al. [27], Su et al. [28], and Fukui et al. [29] demonstrated the influence of pyrolysis temperatue on the electrochemical performance. Two folds can be reached for this system: i) silicon mixed with moderate free-carbon content provides high capacity and cycle ability [30]; and ii) composites show a better performance than pure Si and graphite/graphene, etc. On the other hand, the major challenge facing the Si-based anodes is to achieve good conductivity, structural integrity at work, and cost-effective synthesis, etc [31].

Herein, carbon-rich PDC derived Si/C networks were synthesized via a novel synthesis route using poly(dimethylsilyene)diacetylenes (PDSDA) as single-source-precursor. The structures of Si/Cmaterials were investigated by FTIR, XRD and Raman spectroscopy, suggesting the amorphous to crystalline structure for different pyrolysis temperatures. The capacity of Si/C@800 °C reached as high as 883 mAhg^{-1} at 400 mAg^{-1} with an enhanced capacity retention of 850 mAh·g^{-1} after 500 cycles, *i.e.* 96.3% remaining, creating a new record for PDCs used as anode materials for LIBs. The effects of pyrolysis temperature on the structure suggested that the electrochemical performance of the Si/C ceramic anodes depended on the conductive amorphous carbon network. The Si enhanced the Li ion storage capacity and the carbon served as a conducting source for LIBs. Therefore, the obtained PDCs via pyrolysis was used to estabilsih the relationship between amorphous structure and electrochemical performances, particularly the Li-ion storage properties and possible new advancement in the research field of batteries.

2. Experimetal section

2.1. Materials

An organolithium reagent of n-butyllithium (n-BuLi) (2.5 M), organosilicon compound dimethyldichlorosilane (MSDS, $(CH_3)_2SiCl_2$, purity > 99.5%), hexachloro-1, 3-butadiene (purity > 96%) and trimethylchlorosilane (TCE, $(CH_3)_3SiCl$, purity > 98%) were purchased from Sigma-Aldrich and used as received for the synthesis of poly(dimethylsilylene)diacetylenes (PDSDA). Anhydrous tetrahydrofuran (THF) was distilled from Na/benzophenone under nitrogen.

2.2. Synthesis of PDSDA

Poly(dimethylsilyene)diacetylenes(PDSDA) was synthesized under argon atmosphere according to the published procedures [32]. Briefly, THF (100 mL) and n-BuLi (77.66 g, 0.257 mol) were added into a 500 mL dried flask at −78 °C in an acetone bath. Then, hexachloro-1,3-butadiene (17.271 g, 0.066 mol) was injected through an argon-purged syringe. After continuous shaking, MSDS (8.375 g, 0.065 mol) was added and the temperature was maintained at −78 °C. The reaction was allowed to proceed for one day, and surplus TCE (2 mL) was added into the mixture. PDSDA was obtained after precipitation of their toluene solution in methanol and subsequent evaporating. At last, the PDSDA with a yield of 67% was dried under vacuum for 24 h for further uses in the preparation of anode materials.

2.3. PDSDA derived ceramics

Specified amount of PDSDA was transferred into furnace tube (GSL-1700×, Kejing Co., China) for pyrolysis in Ar atmosphere. The pyrolysis was divided into three steps. First, from 25 to 200 °C, the heating rate was 2 °C min^{-1} and then the temperature was held at 200 °C for 2 h to initiate further cross-linking of the precursor. Second, followed by cross-linking, the temperature was increased to 800, 1000 and 1200 °C for 240 min at a heating rate of 5 K/min. Third, the temperature was gradually decreased to room temperature with a cooling rate of 5 °C/min. The obtained black product was further used as the anode materials and named as Si/C @ 800 °C, Si/C @ 1000 °C and Si/C @ 1200 °C, respectively.

2.4. Cell assembly

The anode was prepared by mixing Si/C active material, polyvinylidene difluoride (PVDF) and acetylene black with a weight ratio of 8:1:1 typically and then ground into slurry with N-methyl kelopyrrolidide (NMP). The Si/C anode material slurry was spread on a high purity copper foil with a scraping blade. The coated copper foil was dried at 80 °C in a vacuum oven overnight. Followed by punching the foil out into individual disk electrodes with a diameter of 16 mm, the electrodes were further dried at 80 °C under vacuum overnight and transferred into glove box. The battery half-cells were assembled with an as-prepared individual disk electrode, a lithium disk (as the reference electrode), a Celgard 2500 film (as separator) and a solution of $LiPF_6$ in ethylene carbonate-dimethyl carbonate (1:1 vol) as the electrolyte in an argon filled glove box. Each half-cell was incubated for 6 h in the glove box before use.

2.5. Characterizations

Fourier transform infrared spectroscopy (FT-IR) was recorded on a Nicolet iSTO spectrometer (Varian, Palo Alto, California, USA) over a range from 4000 to 400 cm^{-1}. The XPS spectra were recorded with a Kratos Axis 165 X-ray photoelectron spectrometer using a monochromatic Al Kα radiation ($h\nu$ = 1486.6 eV) at a take-off angle of 0°. All binding energy values were corrected to C 1s signal (285.0 eV). The

pyrolysis of the samples was investigated by thermogravimetric analysis (TGA) using a thermoanalyzer STA 449 F3 with a heating rate of 10 K/min under argon atmosphere (purity ≥ 99.99%) at a gas flow of 50 mL/min in a temperature range between 40 and 1400 °C. Powder X-ray diffraction (XRD) measurements were carried out on X9Pert Pro Powder diffractometer (Cu Kα radiation, 40 kV, 40 mA) (PANalytical B.V., Netherlands) using crushed sample powders. The X'Celerator scientific RTMS detection unit was used for detection. Scanning electron microscopy (SEM) observations were performed using a VEGA3XMH instrument (Tescan Co., Czech Republic). The EDS mapping of Si/C anode was measured by energy dispersive spectroscopy installed on the SEM. LIR 2025 type coin cells were assembled in the glove box (1220/750/900 Mikrouna, China). Charge-discharge performance of cells was measured galvanostatically at given current densities on LANHE CT2001A (Wuhan, China) multichannel potentiostat. The cyclic voltammetric (CV) and electrochemical impedance spectroscopy (EIS) measurements of the PDC anode were carried out with an AMETEK model 1470E fixed with a 1400 Cell Test System (Solartron analytical).

3. Results and discussion

The Si/C ceramic anode materials were prepared through pyrolysis of PDSDA precursor in a controlled manner. Scheme 1 illustrates the sequential conversion of PDSDA into crosslinking networks and consolidated Si/C linkage and amorphous carbon (ceramic product) after cross-linking and pyrolysis at high temperatures. The thermolysis process of PDSDA was firstly investigated by TGA (Fig. 1a). The weight loss was negligible up to 480 °C, suggesting that PDSDA was stable below 480 °C. Below this temperature, the linear PDSDA was further cross-linked into networks (Scheme 1). Beyond 480 °C, the PDSDA started to decompose gradually and release gases such as H_2, CH_4, and C_2H_4. The total weight loss of PDSDA at 1400 °C was ~16%, owing to the deep cross-linking even at low temperatures and less content of volatile groups in the precursor. Thus, the obtained very high ceramic yield of PDSDA is of great interest for battery industry.

To elucidate the chemical evolution during the pyrolysis, FTIR spectra of PDSDA and Si/C ceramics pyrolyzed at 800, 1000, and 1200 °C have been further investigated (Fig. 1b). After the cross-linking and pyrolysis, the sharp peak of PDSDA at 2080.51 cm^{-1} disappeared because of the formation of Si-C or C-C bonds from ynyl groups in PDSDA [33]. The prominent peak at 800 cm^{-1} correspondes to the Si-C functionalities (SiC_4 tetrahedral species) and the presence of unchanged diacetylenes groups. The peak at 1042.47 cm^{-1} indicates the formation

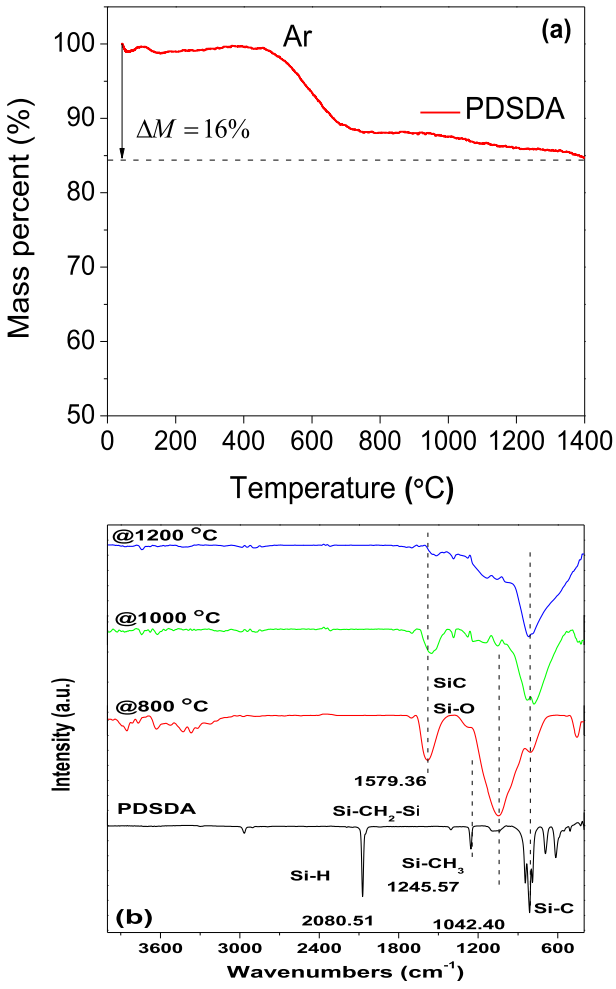

Fig. 1. (a) TGA thermogram of PDSDA determined at a scanning speed of 10 K/min in the presence of argon, (b) FT-IR spectra of: a) PDSDA, b) Si/C @ 800 °C, (c) Si/C @ 1000 °C, and (d) Si/C @ 1200 °C, respectively.

of Si/C ceramic inside an amorphous carbon @ 800 °C [34], owing to the involved only dimethyl-silyl units without functional groups; and the peaks became less intensive with an increased conjugation at higher

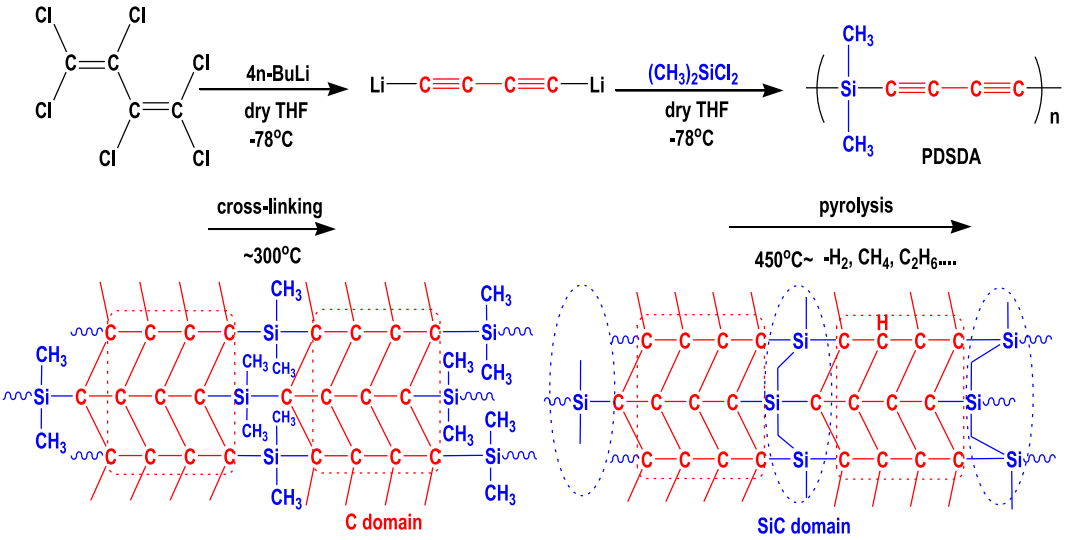

Scheme 1. Progressive conversion of poly(dimethylsilylene diacetylenes) (PDSDA) intocrosslinking networks and consolidated Si/C linkage and amorphous carbon (ceramic product) after cross-linking and pyrolysis at high temperature.

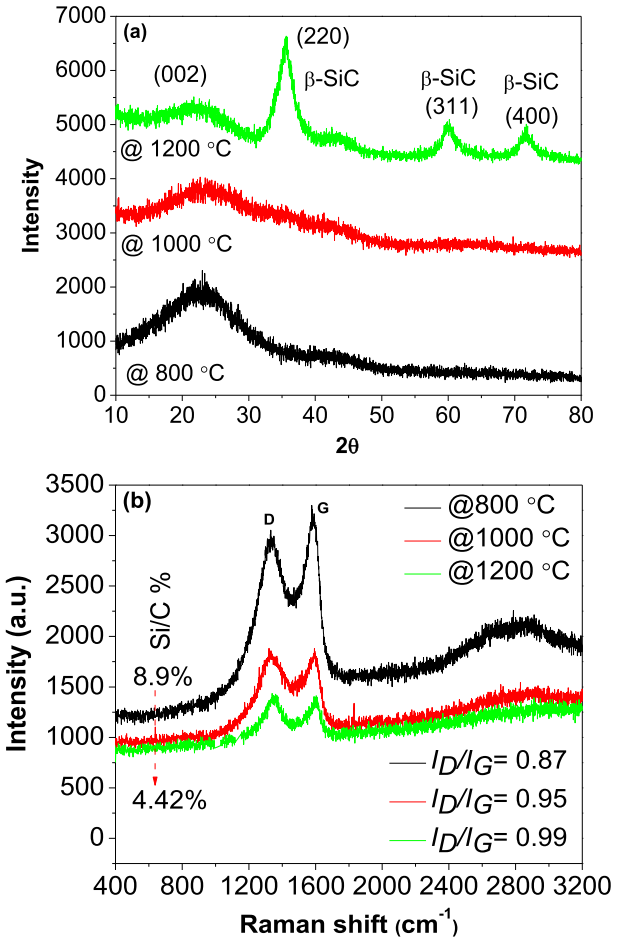

Fig. 2. (a) X-ray diffraction pattern for Si/C anode specimens, confirming the amorphous nature @ (800 °C, 1000 °C and 1200 °C), **(b)** Raman spectra of Si/C, screening facts of D and G bands @ (800 °C, 1000 °C and 1200 °C).

temperatures [35]. By comparison, the broad and more intense small peak at 1245.57 cm^{-1} for Si-CH_3 after pyrolysis confirms the formation of Si-CH_2-Si bond.

To utilize Si/C ceramics as the anode, the crystal structure and composition of C, Si and O could significantly influence the performance. Herein, we measured the XRD to explore the structure evolution of the Si/C ceramics (Fig. 2a). For both Si/C@80 °C and Si/C@1000 °C samples, a broad peak at 23° represents amorphous carbon [36,37]. The prominent peaks at 35.63°, 43.52°, 59.98°, 66.86° and 71.7° suggest the formation of crystalline Si/C phase for the Si/C@1200 °C samples [36]. These characteristic peaks clearly prove the high degree of crystallinity for Si/C@1200 °C. Regarding the Si/C@ 800 °C and Si/C@1000 °C samples, the weak broad peaks at 35.63°, 43.52° and 59.98° suggest the coexistence of amorphous carbon and Si/C structure. With increasing the temperature from 800 to 1200 °C, the carbon structure of pyrolyzed PDSDA involved the evolution from amorphous structure to tetrahedral SiC structure [38]. Consequently, low pyrolysis temperatures brought almost no changes of the original structure but increased the Si phase purity, predicting the beneficial cycling stability performance and Li-ion transformation. The local carbon structure of the Si/C was further investigated by Raman spectroscopy. Fig. 2b shows clear subtle changes of free carbon of the PDC specimens pyrolyzed at different temperatures. The D band at 1334 cm^{-1} arises from the defects of graphitic C structure while the G band at 1577 cm^{-1} consistently increases to 1604 cm^{-1} from amorphous to crystalline structure after pyrolysis [39]. The G band originates from the assortment of D band corresponding to the crystallinity of carbon. Both D and G bands are associated with the disorder-induced characteristics and sp^2 hybridized of carbon atom. The quantitative curve fitting suggested that the relative intensity ratio of D and G band increased from 0.87 to 0.99 with increasing the pyrolysis temperatures, indicating more defects generated and low degree of graphitization [40]. The peak intensity of Si/C @ 800 C increases while the positions of D and G bands shift towards higher wavenumbers at low temperaures. This implies that the electric conductivity of free-carbon phase increases at low temperature and the amorphous level of coating on silicon also increases [41,42]. These defects result from the sp^3 hybrid of SiC structure at a higher

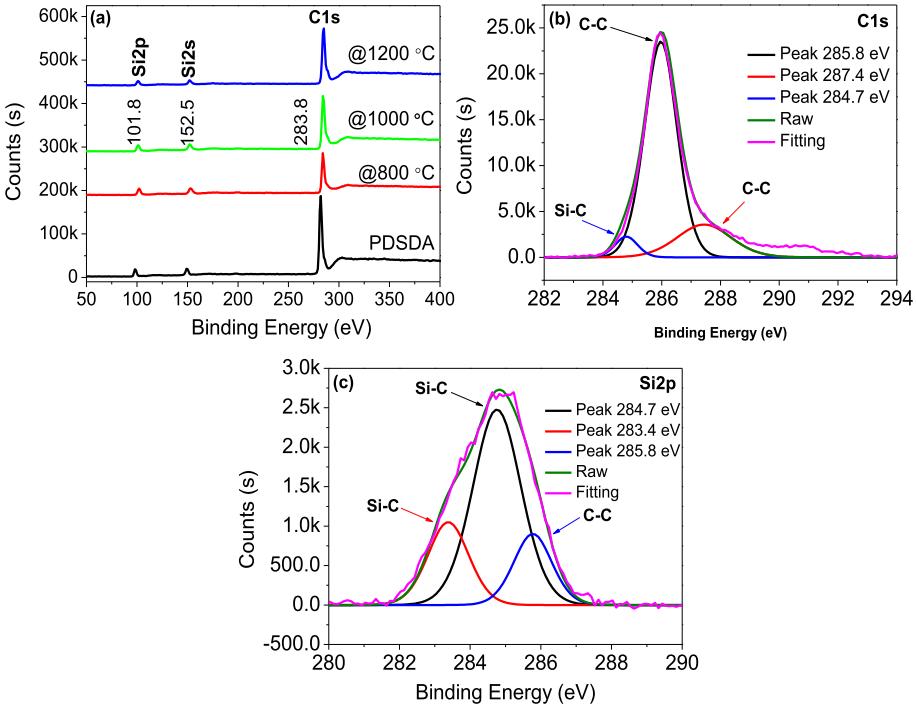

Fig. 3. XPS survey spectra of (a) PDSDA and Si/C @ (800, 1000 and 1200 °C) respectively. High-resolution XPS data and Shirely fitting analysis of Si/C @ 800 °C (b) C1s spectrum, (c) O1s spectrum and (d) Si2p spectrum.

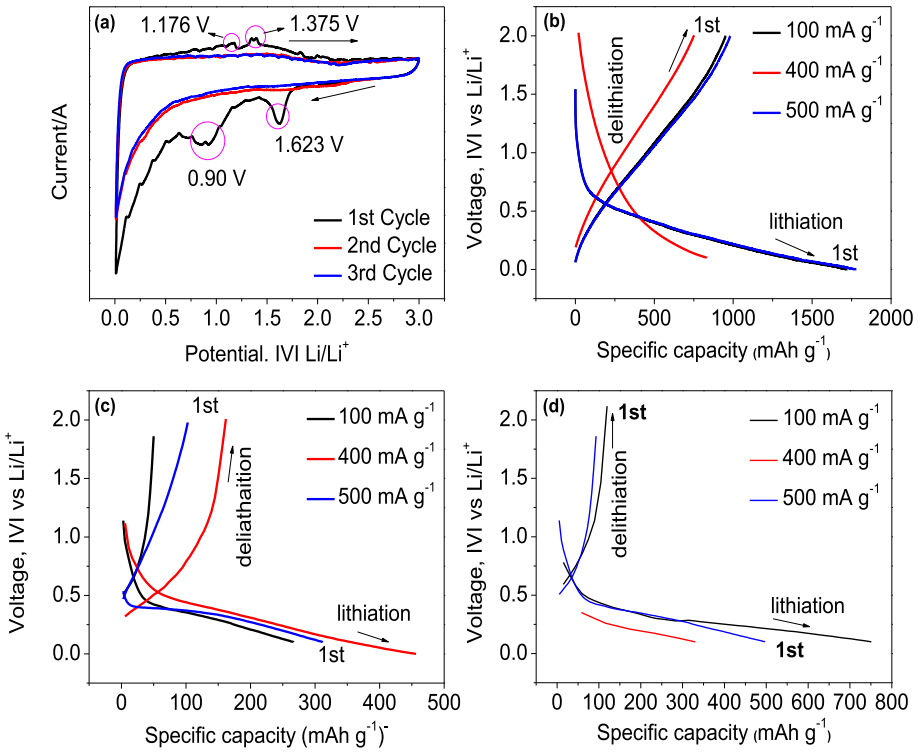

Fig. 4. Specific capacity with respect to cyclic voltammetry at a scan rate of 0.04 mV s^{-1} for (a) Si/C @ 800 °C. Galvano static voltage profiles of 1st and 2nd charge-discharge and corresponding specific capacity for (b) Si/C @ 800 °C, (c) Si/C @ 1000 °C and (d) Si/C @ 1200 °C.

temperature, further confirming the XRD results. The XRD and Raman analysis verified that the Si/C@800 °C sample was mainly composed of amorphous Si and carbon with amorphous Si/C layers as confirmed by the TEM, HRTEM, EDX mapping analysis and their corresponding SAED pattern (Fig. S1, Supporting Information). The structure of Si/C@1000 °C lies between the above two structures. The schematic representing the differentiation of Si/C anode is presented in Fig. S2. The XPS spectra further revealed the presence of Si and C in the PDC matrix (Fig. 3). The content of carbon (80.46%) and silicon (19.54%) confirms that the amorphous rich-carbon coated the silicon particles. Three peaks in C1s spectra at 284.7, 285.8 and 287.4 eV confirmed the formation of SiC and C-C, respectively [43–47]. The deconvoluted Si2p triplets peaks at 283.4, 284.7 and 285.8 eV further prove the formation of Si/C with the C-C Sp^2 bonding. The above peaks confirmed the Si/C bonding in ceramic matrix Si phase and free carbon phase.

The electrochemcial performances of Si/C ceramics have been monitored with the cyclic voltammetry (CV). The CV curves of the Si/C@800 °C sample evidently specified the change of the first cycle from the subsequent cycles (Fig. 4a). The cathodic peaks at 1.623 V vs. Li/Li^+ appeared in the first cycle correspond to the SEI formation during the lithium insertion [48,49], which leads to a low coulombic efficiency and irreversible capacity. The cathodic peak at 0.90 V vs. Li/Li^+ is attributed to the formation of Li_xSi_y. While the anodic peaks at 1.176 and 1.375 V vs Li/Li^+ represent the delithiation reaction of Li_xSi_y [49]. The differences between the first and subsequential cycles were ascribable to the decompositioon of organic electrolyte to form SEI. The reproducible second and third cycles suggest the good cycling stability of Si/C anode.

To examine the performance of half-cell, the charge/discharge capacities of the Si/C ceramic anode and lithium foil as commercial cathode in $LiPF_6$ have been further investigated. The first discharge capacity of Si/C@800 °C at 100 mAg^{-1} was 1732.2 $mAhg^{-1}$ and dropped to 901 $mAhg^{-1}$ in the second cycle, while at a higher current density of 500 mAg^{-1}, the first discharge capacity was 1780.2 $mAh{\cdot}g^{-1}$ and decreased to 981.3 $mAh{\cdot}g^{-1}$ in the next cycle, thus resulting in a first cycle loss of 44%. While the charge capacities for the Si/C@1000 °C and Si/C@1200 °C samples at the corresponding current densities in the first cycle were 63.0 and 137.0 $mAhg^{-1}$, causing a high first cycle loss of 76.36% and 81.75% in capacity. A high first cycle loss was observed due to the quick parasitic reactions at high voltage, and this loss could be reduced by activating the cell before charge/discharge at a low current rate [50].

In Fig. 4b, the Si/C@800 °C sample showed a better capacity retention of 90.32% in the first cycle at 400 mAg^{-1} and a higher coulombic efficiency of 90% compared to the Si/C@1000 °C sample (35.48%) and the Si/C@1200 °C sample (31.56%) at the identical current density (Fig. 4c and d). This low capacity retention of Si/C @1000 °C and Si/C @ 1200 °C originated from the formation of stable SEI layer by reacting with electrolyte in the first few cycles in the range of 0.1–2.0 V [48]. The charge curve was at 2.0 V while the discharge measurements started at 1.15 V because the cell was subjected to the state of rest at the charge position during electrochemical cycling test. This difference in the voltage hysteresis was observed due to the holding time of the anode and/or designated to fewer irreversible insertion sites for the Li ions in the anode material [51]. To the best of our knowledge, the charge and discharge capacities of ~752.1 and ~832.7 $mAhg^{-1}$ at 400 mAg^{-1} for Si/C@800 °C presented more remarkable yielding capacity retention as high as 90.32%, which outperformed the previously reported PDCs [52]. The larger first insertion and extraction capacities of the Si/C@800 °C sample suggested more available ion insertion sites. Considering the capacities of Si/C@1000 °C and Si/C@1200 °C anodes, the first two cycles loss mechanism depends significantly on the Si/C structure which was in close agreement with the results reported on the SiCN and SiOC ceramics [22,53].

The structural features of Si/C matrix influence the extended cycling performance with varying current densities (Fig. 5). The reversible capacity at 170 mAg^{-1} reaches the largest value, yielding ~677.87 $mAhg^{-1}$ for the Si/C@800 °C sample, ~349.05 $mAhg^{-1}$ for the Si/C@1000 °C sample and ~279.79 $mAhg^{-1}$ for the Si/C@1200 °C sample. The Si/C@800 °C sample thus achieved the highest capacity, further

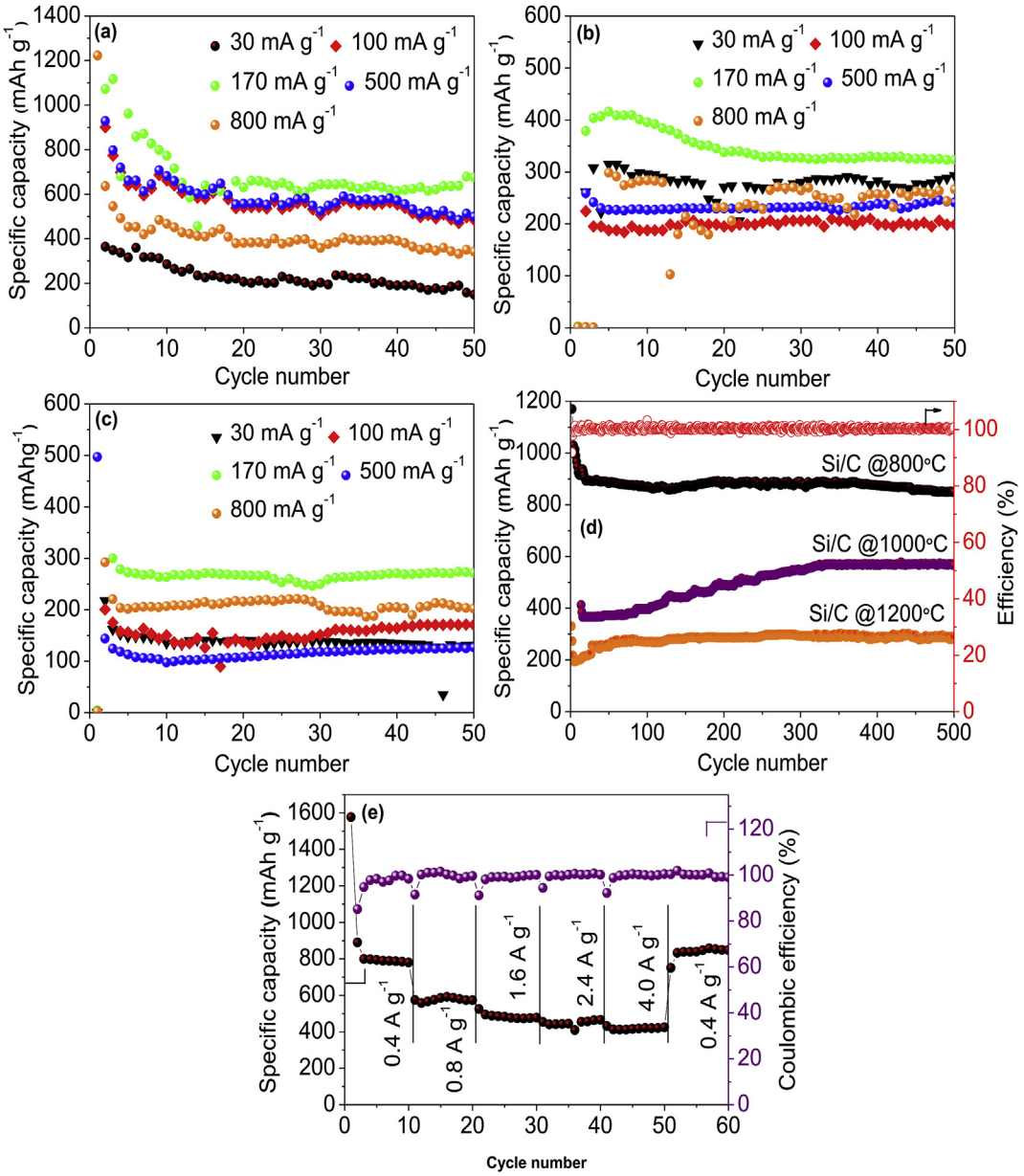

Fig. 5. Cycle life competence for (a) Si/C @ 800 °C, (b) Si/C @ 1000 °C and (c) Si/C @ 1200 °C at various current densities; (Average CE of Si/C @ 800 °C associated to respective anodes; (d) prolonged cycling competence of various as-prepared Si/C anodes at 400 mA·g^{-1}and (e) rate test and coulombic efficiency for Si/C @ 800 °C at different current densities. A cut-off voltage range is 0.001–2.0 V vs. Li/Li^{+}.

confirming the first cycle electrochemical performance as shown in Fig. 4a–c. This might be ascribed to the inferior irreversible capacity and improved interface kinetics because of the enhanced coulombic efficiency [54–66]. At a relatively high current density of 400 mAg^{-1} (Fig. 5d), the Si/C@800 °C sample exhibited the highest capacity value of ~883 mAhg^{-1} and its retention could reach as high as 90% after even 500 cycles. This arises from the amorphous carbon shell being well-connected with Si, which both accommodated the volume expansion and served as electrical conducting pathway. Moreover, the high capacity retention was attributed to the SEI formation at the ceramic surface during the lithiation and delithiation, preventing the pulverization of the Si. The cycled Si/C@800 °C sample after 500 cycles showed almost no pulverization (Fig. S4d), no noticed surface cracks indicate a stable cycling with minor deviations. Fig. 5e shows the steady rate performance of the Si/C@800 °C sample. When increasing from 0.4 to 4.0 Ag^{-1}, the capacity changed from ~880 to ~419 mAhg^{-1}. After 60 cycles at 0.4 Ag^{-1}, the capacity of Si/C@800 °C still retained 835.46 mAhg^{-1}, indicating excellent rate performance of the Si/C@800 °C anode with > 99% coulombic efficiency. Here, the superior cycling durability, coulombic efficiency and rate performance of the Si/C@800 °C sample are due to the presence of amorphous Si/C in the ceramic matrix behaving as the lithium storage sites, whereas the PDSDA pyrolyzed at high temperatures formed crystalline SiC domains with saturated tetrahedral configuration, resulting in low bonding sites for lithium ions. The evolution of these structures with temperatures was confirmed by XRD, Raman and XPS results. Thus, the electrochemical performance depended essentially on the structures of the Si/C ceramic materials.

The temperature performance is of great importance for battery industry. Most researches focused on the electrolyte and the performance of anode materials towards lower freezing point and higher conductivity [67–69]. The Si/C @ 800 °C anode even at −5 °C revealed a charge capacity of ~347 mAhg^{-1} at 400 mA g^{-1}with almost an average coulombic efficiency of 74% (Fig. 6). The rate to transport

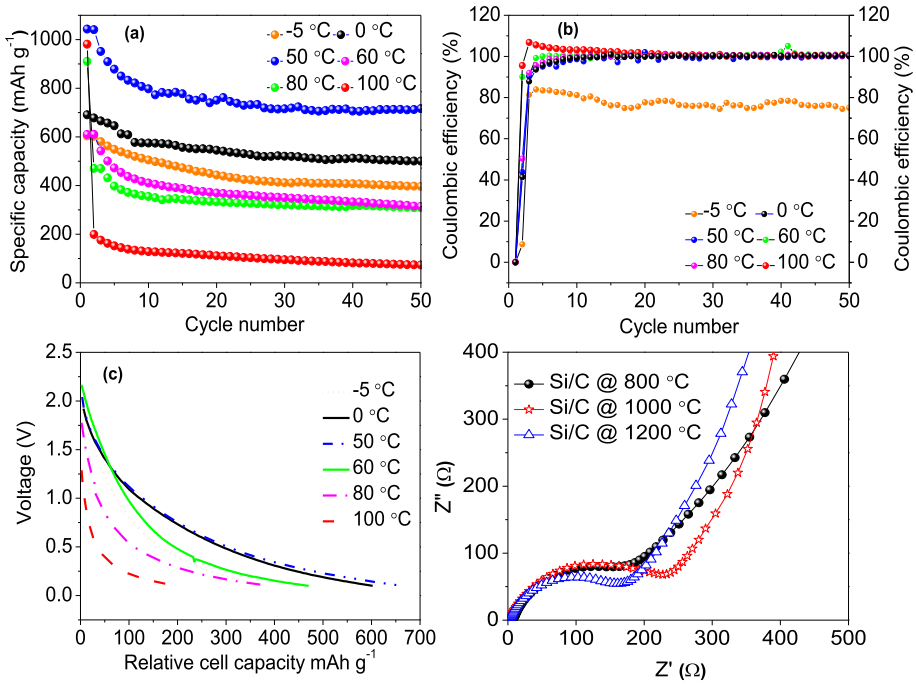

Fig. 6. The performance of Si/C @ 800 °C anode at 400 mA g^{-1}: (a) specific capacity, (b) coulombic efficiency (%), (c) discharge curves at low and high temperatures and (d) electrochemical impedance spectra of as-prepared Si/C anodes @ various temperatures.

active chemicals is reduced with decreasing the working temperature, leading to a reduction in the power charge capacity of the battery. The reduced operational voltage from 2.0 to 0.1 V at −5 °C could be attributed to an improved plug-in polarization of the Si/C anode owing to the shrinkage in the conductivity of $LiPF_6$ and SEI formation. Thus, the Li-ion diffusion coefficient (D_{Li}) directly depends on the temperature, following the Arrhenius equation [69]. At relatively higher temperatures, the charge capacity was decreased to ~124 mAh g^{-1} at 400 mA g^{-1} beyond 80 °C. The cell charge capacity decreases with increasing the temperature over the range between 50 and 100 °C. The coulombic efficiency still retained nearly 99% at higher temperatures. The loss in capacity arose from the breakdown of SEI layer due to the physical penetration. Interestingly, the discharge curves of the Si/C @ 800 °C sample (Fig. 6c) were comparable at various temperatures, suggesting high stability and adaptability with temperature variations.

The electrochemical impedance (EIS) was tested to further investigate the performance of Si/C anodes (Fig. 6d). All EIS spectra consist of a depressed semicircle from high to medium frequencies correlated to the SEI and charge transfer impedance (R_{ct}), while an inclined line at high to low frequencies is attributed to the good ion diffusion inside the anode [70]. The R_{ct} of the Si/C@ 800 °C sample (145 Ω) was always smaller than that of the Si/C@1000 °C sample (227 Ω) and the Si/C@ 1200 °C sample (161 Ω), respectively. The results indicated that the Si/C@800 °C sample had a high electrical conductivity and was propitious to lithium ion diffusion. Those findings have further proved the largest capacity and best stability in case of the Si/C@ 800 °C sample.

4. Conclusions

A novel and cost-effective route was used to prepare the PDSDA-derived Si/C ceramics. The resultant PDSDA-derived Si/C ceramic anodes revealed enhanced Li-ion storage aptitude, specific capacity and stable cycling by electrochemical test. This structure-based performance was mainly caused by the evolution of Si/C matrix from amorphous to crystalline structure. The resulting Si/C@800 °C sample exhibited a high specific capacity ~883 mAh g^{-1} at 400 mA g^{-1}, with > 99% coulombic efficiency (CE), and 90% capacity retention even after 500 cycles, setting a new record for PDC anode materials in the LIBs. Furthermore, higher charge/discharge performance was correlated to the Si/C ultra-sp^2 structure due to the amorphous Si/C formation that took place inside the ceramic matrix. This unique structure and component accommodated the volume expansion, increased the conductivity, and avoided the electrode liquidation. In addition, this Si/C ceramics anode preparation is inexpensive, accessible and applicable to other high ceramic electrode materials. This study proposed a feasible method to utilize Si/C ceramics in large-scale serving as the high-performance anodes for next-generation lithium ion batteries.

Notes

The authors declare no competing financial interest.

Acknowledgements

The authors acknowledge financial support from the National Natural Science Foundation of China (21174112) and (21703172), Fundamental Research Funds for the Central Universities (3102015BJ (II)JGZ026), the State Key Laboratory of Solidification Processing in NWPU (SKLSP201629), Shaanxi Natural Science Foundation of Shaanxi Province (2016JQ2013). The authors acknowledge the financial support of CSC Scholarship Graduate Program (2015GXZ039; 2016GXYF32). Q. G. was supported as part of the Fluid Interface Reactions, Structures and Transport (FIRST) Center, an Energy Frontier Research Center funded by the U.S. Department of Energy, Office of Science, Office of Basic Energy Sciences. A portion of this research was conducted at the Center for Nanophase Materials Sciences, which is a DOE Office of Science User Facility.

Appendix A. Supplementary data

Supplementary data to this article can be found online at https://doi.org/10.1016/j.ceramint.2019.02.123.

References

[1] Y. Sun, N. Liu, Y. Cui, Promises and challenges of nanomaterials for lithium-based rechargeable batteries, Nature Energy 1 (2016) 16071.
[2] J.R. Szczech, S. Jin, Nanostructured silicon for high capacity lithium battery anodes, Energy Environ. Sci. 4 (2011) 56–72.
[3] L. David, S. Bernard, C. Gervais, P. Miele, G. Singh, Facile synthesis and high rate capability of silicon carbonitride/boron nitride composite with a sheet-like morphology, J. Phys. Chem. C 119 (2015) 2783–2791.
[4] H.T. Nguyen, F. Yao, M.R. Zamfir, C. Biswas, K.P. So, Y.H. Lee, S.M. Kim, S.N. Cha, J.M. Kim, D. Pribat, Highly interconnected Si nanowires for improved stability Li-ion battery anodes, Adv. Energy Mater. 1 (2011) 1154–1161.
[5] H. Wu, G. Chan, J.W. Choi, I. Ryu, Y. Yao, M.T. McDowell, S.W. Lee, A. Jackson, Y. Yang, L. Hu, Y. Cui, Stable cycling of double-walled silicon nanotube battery anodes through solid–electrolyte interphase control, Nat. Nanotechnol. 7 (2012) 310.
[6] K. Yan, Z. Lu, H.W. Lee, F. Xiong, P.C. Hsu, Y. Li, J. Zhao, S. Chu, Y. Cui, Selective deposition and stable encapsulation of lithium through heterogeneous seeded growth, Nature Energy 1 (2016) 16010.
[7] J.I. Lee, N.S. Choi, S. Park, Highly stable Si-based multicomponent anodes for practical use in lithium-ion batteries, Energy Environ. Sci. 5 (2012) 7878–7882.
[8] J.I. Lee, K.T. Lee, J. Cho, J. Kim, N.S. Choi, S. Park, Chemical-assisted thermal disproportionation of porous silicon monoxide into silicon-based multicomponent systems, Angew. Chem. Int. Ed. 51 (2012) 2767–2771.
[9] R. Yi, F. Dai, M.L. Gordin, S. Chen, D. Wang, Micro-sized Si-C composite with interconnected nanoscale building blocks as high-performance anodes for practical application in lithium-ion batteries, Adv. Energy Mater. 3 (2013) 295–300.
[10] V. Liebau-Kunzmann, C. Fasel, R. Kolb, R. Riedel, Lithium containing silazanes as precursors for SiCN: Li ceramics—a potential material for electrochemical applications, J. Eur. Ceram. Soc. 26 (2006) 3897–3901.
[11] J. Kaspar, G. Mera, A.P. Nowak, M. Graczyk-Zajac, R. Riedel, Electrochemical study of lithium insertion into carbon-rich polymer-derived silicon carbonitride ceramics, Electrochim. Acta 56 (2010) 174–182.
[12] M. Graczyk-Zajac, G. Mera, J. Kaspar, R. Riedel, Electrochemical studies of carbon-rich polymer-derived SiCN ceramics as anode materials for lithium-ion batteries, J. Eur. Ceram. Soc. 30 (30) (2010) 3235–3243.
[13] R. Bhandavat, G. Singh, Improved electrochemical capacity of precursor-derived Si (B) CN-carbon nanotube composite as Li-ion battery anode, ACS Appl. Mater. Interfaces (2012) 45092–45097.
[14] W. Deng, T. Kang, H. Liu, J. Zhang, N. Wang, N. Lu, Y. Ma, A. Umar, Z. Guo, Potassium hydroxide activated and nitrogen doped graphene with enhanced supercapacitive behavior, Sci. Adv. Mater. 10 (2018) 937–949.
[15] W. Du, X. Wang, J. Zhan, X. Sun, L. Kang, F. Jiang, X. Zhang, Q. Shao, M. Dong, H. Liu, V. Murugadoss, Biological cell template synthesis of nitrogen-doped porous hollow carbon spheres/MnO2 composites for high-performance asymmetric supercapacitors, Electrochim. Acta 296 (2019) 907–915.
[16] M. Liu, Q. Meng, Z. Yang, X. Zhao, T. Liu, Ultra-long-term cycling stability of an integrated carbon–sulfur membrane with dual shuttle-inhibiting layers of graphene “nets” and a porous carbon skin, Chem. Comm. 54 (2018) 5090–5093.
[17] R. Li, X. Zhu, Q. Fu, G. Liang, Y. Chen, L. Luo, M. Dong, Q. Shao, R. Wei, C. Lin, Z. Guo, Nanosheet-based $Nb_{12}O_{29}$ hierarchical microspheres for enhanced lithium storage, Chem. Comm. (2019), https://doi.org/10.1039/C8CC09924C in press.
[18] H. Du, C.X. Zhao, J. Lin, J. Guo, B. Wang, Z. Hu, Q. Shao, D. Pan, E.K. Wujcik, Z. Guo, Carbon nanomaterials in direct liquid fuel cells, Chem. Rec. 18 (2018) 1365–1372.
[19] M. Liu, B. Li, H. Zhou, C. Chen, Y. Liu, T. Liu, Extraordinary rate capability achieved by a 3D “skeleton/skin” carbon aerogel–polyaniline hybrid with vertically aligned pores, Chem. Comm. 53 (2017) 2810–2815.
[20] C. Wang, Z. He, X. Xie, X. Mai, Y. Li, T. Li, M. Zhao, C. Yan, H. Liu, E. Wujcik, Z. Guo, Controllable cross-linking anion exchange membranes with excellent mechanical and thermal properties, Macromol. Mater. Eng. 3 (2018) 1700462.
[21] S. Choi, D.S. Jung, J.W. Choi, Scalable fracture-free SiOC glass coating for robust silicon nanoparticle anodes in lithium secondary batteries, Nano Lett. 14 (2014) 7120–7125.
[22] L. David, R. Bhandavat, U. Barrera, G. Singh, Silicon oxycarbide glass-graphene composite paper electrode for long-cycle lithium-ion batteries, Nat. Comm. 7 (2016) 10998.
[23] M. Halim, C. Hudaya, A.Y. Kim, J.K. Lee, Phenyl-rich silicone oil as a precursor for SiOC anode materials for long-cycle and high-rate lithium ion batteries, J. Mater. Chem. 4 (2016) 2651–2656.
[24] D. Vrankovic, M. Graczyk-Zajac, C. Kalcher, J. Rohrer, M. Becker, C. Stabler, G. Trykowski, K. Albe, R. Riedel, Highly porous silicon embedded in a ceramic matrix: a stable high-capacity electrode for Li-ion batteries, ACS Nano 11 (2017) 11409–11416.
[25] M. Graczyk-Zajac, C. Fasel, R. Riedel, Polymer-derived-SiCN ceramic/graphite composite as anode material with enhanced rate capability for lithium ion batteries, J. Power Sour. 196 (2011) 6412–6418.
[26] Y. Feng, N. Feng, Y. Wei, Y. Bai, Preparation and improved electrochemical performance of SiCN–graphene composite derived from poly (silylcarbondiimide) as Li-ion battery anode, J. Mater. Chem. A. 2 (2014) 4168–4177.
[27] J. Kaspar, M. Graczyk-Zajac, R. Riedel, Lithium insertion into carbon-rich SiOC ceramics: influence of pyrolysis temperature on electrochemical properties, J. Power Sour. 244 (2013) 450–455.
[28] D. Su, Y.L. Li, Y. Feng, J. Jin, Electrochemical properties of polymer-derived SiCN materials as the anode in lithium ion batteries, J. Am. Ceram. Soc. 92 (2009) 2962–2968.
[29] H. Fukui, K. Eguchi, H. Ohsuka, T. Hino, K. Kanamura, Structures and lithium storage performance of Si–O–C composite materials depending on pyrolysis temperatures, J. Power Sour. 243 (2013) 152–158.
[30] S. Mukherjee, Z. Ren, G. Singh, Molecular polymer-derived ceramics for applications in electrochemical energy storage devices, J. Phys. D Appl. Phys. 51 (2018) 463001.
[31] D.A. Agyeman, K. Song, G.H. Lee, M. Park, Y.M. Kang, Carbon-coated Si nanoparticles anchored between reduced graphene oxides as an extremely reversible anode material for high energy-density Li-ion battery, Adv. Energy Mater. 6 (2016) 1600904.
[32] R.J. Corriu, C. Guerin, B. Henner, A. Jean, H. Mutin, Organosilicon polymers: pyrolysis of poly [(silanylene) diethynylene] s, J. Organomet. Chem. 396 (1990) C35–C38.
[33] M.I. Lipschutz, T. Chantarojsiri, Y. Dong, T.D. Tilley, Synthesis, characterization, and alkyne trimerization catalysis of a heteroleptic two-coordinate FeI complex, J. Am. Chem. Soc. 137 (2015) 6366–6672.
[34] G. Ramis, P. Quintard, M. Cauchetier, G. Busca, V. Lorenzelli, Surface chemistry and structure of ultrafine silicon carbide: an FT-IR study, J. Am. Ceram. Soc. 72 (1989) 1692–1697.
[35] R.J. Corriu, P. Gerbier, C. Guerin, B.J. Henner, A. Jean, P.H. Mutin, Organosilicon polymers: pyrolysis chemistry of poly [(dimethylsilylene) diacetylene], Organometallics 11 (1992) 2507–2513.
[36] W. Ren, Y. Wang, Z. Zhang, Q. Tan, Z. Zhong, F. Su, Carbon-coated porous silicon composites as high performance Li-ion battery anode materials: can the production process be cheaper and greener? J. Mater. Chem. A. 4 (2016) 552–560.
[37] C.W. Hoge, D. McGurk, J.L. Thomas, A.L. Cox, C.C. Engel, C.A. Castro, Mild traumatic brain injury in US soldiers returning from Iraq, N. Engl. J. Med. 358 (2008) 453–463.
[38] D. Ahn, R. Raj, Thermodynamic measurements pertaining to the hysteretic intercalation of lithium in polymer-derived silicon oxycarbide, J. Power Sour. 195 (2010) 3900–3906.
[39] M.V. Shelke, H. Gullapalli, K. Kalaga, M.T. Rodrigues, R.R. Devarapalli, R. Vajtai, P.M. Ajayan, Facile synthesis of 3D anode assembly with Si nanoparticles sealed in highly pure few layer graphene deposited on porous current collector for long life Li-ion battery, Adv. Mater. Interf. 4 (2017) 1601043.
[40] Y. Huangfu, C. Liang, Y. Han, H. Qiu, P. Song, L. Wang, J. Kong, J. Gu, Fabrication and investigation on the Fe3O4/thermally annealed graphene aerogel/epoxy electromagnetic interference shielding nanocomposites, Compos. Sci. Technol. 169 (2019) 70–75.
[41] J. Ru, Y. Fan, W. Zhou, Z. Zhou, T. Wang, R. Liu, J. Yang, X. Lu, J. Wang, C. Ji, L. Wang, Electrically conductive and mechanically strong graphene/mullite ceramic composites for high-performance electromagnetic interference shielding, ACS Appl. Mater. Interfaces 10 (2018) 39245–39256.
[42] Y. Yoshida, Y. Ishii, N. Kato, C. Li, S. Kawasaki, Low-temperature phase transformation accompanied with charge-transfer reaction of polyiodide ions encapsulated in single-walled carbon nanotubes, J. Phys. Chem. C 120 (2016) 20454–20461.
[43] S. Batool, M. Idrees, Q. Hussain, J. Kong, Adsorption of copper (II) by using derivedfarmyard and poultry manure biochars: efficiency and mechanism, Chem. Phys. Lett. 689 (2017) 190–198.
[44] M. Idrees, S. Batool, Q. Hussain, H. Ullah, M.I. Al-Wabel, M. Ahmad, J. Kong, High efficiency remediation of cadmium (Cd^{2+}) from aqueous solution using poultry manure–and farmyard manure–derived biochars, Separ. Sci. Technol. 51 (2016) 2307–2317.
[45] M. Idrees, S. Batool, H. Ullah, Q. Hussain, M.I. Al-Wabel, M. Ahmad, A. Hussain, M. Riaz, Y.S. Ok, J. Kong, Adsorption and thermodynamic mechanisms of manganese removal from aqueous media by biowaste-derived biochars, J. Mol. Liq. 266 (2018) 373–380.
[46] M. Idrees, S. Batool, T. Kalsoom, S. Yasmeen, A. Kalsoom, S. Raina, Q. Zhuang, J. Kong, Animal manure-derived biochars produced via fast pyrolysis for the removal of divalent copper from aqueous media, J. Environ. Manag. 213 (2018) 109–118.
[47] S. Batool, M. Idrees, M.I. Al-Wabel, M. Ahmad, K. Hina, H. Ullah, L. Cui, Q. Hussain, Sorption of Cr(III) from aqueous media via naturally functionalized microporous biochar: mechanistic study, Microchem. J. 144 (2019) 242–253.
[48] K. Saravanan, M. Nagarathinam, P. Balaya, J.J. Vittal, Lithium storage in a metal organic framework with diamondoid topology–A case study on metal formates, J. Mater. Chem. 20 (2010) 8329–8335.
[49] A.J. Gmitter, I. Plitz, G.G. Amatucci, High concentration dinitrile, 3-alkoxypropionitrile, and linear carbonate electrolytes enabled by vinylene and monofluoroethylene carbonate additives, J. Electrochem. Soc. 159 (2012) A370–A379.
[50] M. Idrees, S. Batool, J. Kong, et al., Polyborosilazane derived ceramics-nitrogen sulfur dual doped graphene nanocomposite anode for enhanced lithium ion batteries, Electrochim. Acta 296 (2019) 925–937.
[51] D. Su, Y.L. Li, Y. Feng, J. Jin, Electrochemical properties of polymer-derived SiCN materials as the anode in lithium ion batteries, J. Am. Ceram. Soc. 92 (2009) 2962–2968.
[52] F. Ji, Y.L. Li, J.M. Feng, D. Su, Y.Y. Wen, Y. Feng, F. Hou, Electrochemical performance of graphene nanosheets and ceramic composites as anodes for lithium batteries, J. Mater. Chem. 19 (2009) 9063–9067.
[53] D. Ahn, R. Raj, Cyclic stability and C-rate performance of amorphous silicon and carbon based anodes for electrochemical storage of lithium, J. Power Sour. 196 (2011) 2179–2186.
[54] P. Dibandjo, M. Graczyk-Zajac, R. Riedel, V.S. Pradeep, G.D. Soraru, Lithium insertion into dense and porous carbon-rich polymer-derived SiOC ceramics, J. Eur. Ceram. Soc. 32 (2012) 2495–2503.

[55] J. Tian, Q. Shao, X. Dong, J. Zheng, D. Pan, X. Zhang, H. Cao, L. Hao, J. Liu, Z. Guo, Bio-template synthesized NiO/C hollow microspheres with enhanced Li-ion battery electrochemical performance, Electrochim. Acta 261 (2018) 236–245.
[56] M. Liu, Z. Yang, H. Sun, C. Lai, X. Zhao, H. Peng, T. Liu, A hybrid carbon aerogel with both aligned and interconnected pores as interlayer for high-performance lithium–sulfur batteries, Nano Res 9 (2016) 3735–3746.
[57] M. Liu, Q. Meng, Z. Yang, X. Zhao, T. Liu, Ultra-long-term cycling stability of an integrated carbon-sulfur membrane with dual shuttle-inhibiting layers of graphene "nets" and a porous carbon skin, Chem. Comm 54 (2018) 5090–5093.
[58] C. Wang, B. Mo, Z. He, Q. Shao, D. Pan, E. Wujick, J. Guo, X. Xie, X. Xie, Z. Guo, Crosslinked norbornene copolymer anion exchange membrane for fuel cells, J. Membr. Sci. 556 (2018) 118–125.
[59] C. Hou, Z. Tai, L. Zhao, Y. Zhai, Y. Hou, Y. Fan, F. Dang, J. Wang, H. Liu, High performance MnO@C microcages with a hierarchical structure and tunable carbon shell for efficient and durable lithium storage, J. Mater. Chem. 6 (2018) 9723–9736.
[60] (a) Z. Qu, M. Shi, H. Wu, Y. Liu, J. Jiang, C. Yan, An efficient binder-free electrode with multiple carbonized channels wrapped by $NiCo_2O_4$ nanosheets for high-performance capacitive energy storage, J. Power Sources 410 (2019) 179–187;
(b) C. Wang, F. Lan, Z. He, X. Xie, Y. Zhao, H. Hou, L. Guo, V. Murugadoss, H. Liu, Q. Shao, Q. Gao, T. Ding, R. Wei, Z. Guo, Iridium-based catalysts for solid polymer electrolyte electrocatalytic water splitting, Chemsuschem (2019) in press https://doi.org/10.1002/cssc.201802873.
[61] Y. Jiao, J. Zhang, S. Liu, Y. Liang, S. Li, H. Zhou, J. Zhang, The graphene oxide ionic solvent-free nanofluids and their battery performances, Sci. Adv. Mater. 10 (2018) 1706–1713.
[62] B. Kirubasankar, V. Murugadoss, J. Lin, T. Ding, M. Dong, H. Liu, J. Zhang, T. Li, N. Wang, Z. Guo, S. Angaiah, In situ grown nickel selenide on graphene nanohybrid electrodes for high energy density asymmetric supercapacitors, Nanoscale 10 (2018) 20414–20425.
[63] W. Zhao, X. Li, R. Yin, L. Qian, X. Huang, H. Liu, J. Zhang, J. Wang, T. Ding, Z. Guo, Urchin-like NiO–NiCo 2 O 4 heterostructure microsphere catalysts for enhanced rechargeable non-aqueous Li–O 2 batteries, Nanoscale 11 (2019) 50–59.
[64] X. Lou, C. Lin, Q. Luo, J. Zhao, B. Wang, J. Li, Q. Shao, X. Guo, N. Wang, Z. Guo, Crystal structure modification enhanced FeNb11O29 anodes for lithium-ion batteries, ChemElectroChem 4 (2017) 3171–3180.
[65] C. Lin, L. Hu, C. Cheng, K. Sun, X. Guo, Q. Shao, J. Li, N. Wang, Z. Guo, Nano-TiNb2O7/carbon nanotubes composite anode for enhanced lithium-ion storage, Electrochim. Acta 260 (2018) 65–72.
[66] Q. Hou, J. Ren, H. Chen, P. Yang, Q. Shao, M. Zhao, X. Zhao, H. He, N. Wang, Q. Luo, Z. Guo, Synergistic hematite-fullerene electron-extracting layers for improved efficiency and stability in perovskite solar cells, ChemElectroChem 5 (2018) 726–731.
[67] M.J. Mühlbauer, O. Dolotko, M. Hofmann, H. Ehrenberg, A. Senyshyn, Effect of fatigue/ageing on the lithium distribution in cylinder-type Li-ion batteries, J. Power Sour. 348 (2017) 145–149.
[68] C.K. Huang, J.S. Sakamoto, J. Wolfenstine, S. Surampudi, The limits of low--temperature performance of Li-ion cells, J. Electrochem. Soc. 147 (2000) 2893–2896.
[69] C. Wang, A.J. Appleby, F.E. Little, Low-temperature characterization of lithium-ion carbon anodes via microperturbation measurement, J. Electrochem. Soc. 149 (2002) A754–A760.
[70] H. Zhang, Q. Deng, A. Zhou, X. Liu, J. Li, Porous Li 2 C 8 H 4 O 4 coated with N-doped carbon by using CVD as an anode material for Li-ion batteries, J. Mater. Chem. A. 2 (2014) 5696–5702.